Revista de la Academia Colombiana de Ciencias Exactas, Físicas y Naturales. 2025
doi: https://doi.org/10.18257/raccefyn.3225

Physical sciences

Original article

Study of the structural and optical properties of $CuInSe_2$ thin films obtained by RF sputtering as a function of the deposition temperature

Estudio de las propiedades estructurales y ópticas de películas delgadas de $CuInSe_2$ obtenidas mediante pulverización catódica por radiofrecuencia en función de la temperatura de depósito

Jorge Montes-Monsalve[1,*], Roberto Bernal-Correa[2], Arturo Morales-Acevedo[3], Álvaro Pulzara-Mora[4]

[1] Dirección Académica, Universidad Nacional de Colombia, Sede de La Paz, La Paz, Cesar, Colombia
[2] Instituto de Estudios de la Orinoquia, Universidad Nacional de Colombia, Arauca, Colombia
[3] Centro de Investigación y de Estudios Avanzados del IPN, Departamento de Ingeniería Eléctrica-SEES, Ciudad de México, México
[4] Laboratorio de Nanoestructuras Semiconductoras, Universidad Nacional de Colombia, Sede Manizales, Colombia

Abstract

The formation of a copper-deficient surface layer is a common phenomenon in $CuInSe_2$ thin films, typically arising in deposition processes that involve multiple steps, such as thermal treatment and post-selenization. Here, we studied the radio-frequency magnetron sputtering film deposition from a $CuInSe_2$ target. Substrate temperature varied between 50 and 400°C. X-ray photoelectron spectroscopy (XPS) confirmed the persistent presence of a Cu-deficient surface layer across all deposition temperatures. Films grown below 200°C were amorphous and Cu-deficient, while at 200°C and above, the films exhibited a transition to a polycrystalline chalcopyrite structure, as evidenced by X-ray diffraction (XRD). The crystallite size for the polycrystalline films deposited at 200°C and 400°C was approximately 10–12 nm. Energy dispersive spectroscopy (EDS) revealed a progressive decrease in copper content from ~20 at.% at 50–200°C to ~16 at.% at 400°C, while indium remained nearly constant and selenium increased slightly from 50 at.% to 56 at.% with increasing temperature. UV-Vis spectroscopy showed that the optical bandgap (E_g) decreased from 1.2 eV at 50°C and 1.15 eV at 100°C to approximately 0.95–0.94 eV at 200°C and 400°C. Our results provide valuable insights into the effect of substrate temperature on $CuInSe_2$ thin films, contributing to the ongoing efforts to optimize their properties for photovoltaic and optoelectronic applications.

Keywords: Copper indium selenide; Thin film; X-ray photo-electron spectroscopy; Raman spectroscopy; X-ray diffraction; Optoelectronic; Photovoltaic.

Resumen

La formación de una capa superficial deficiente en cobre es una característica común en las películas delgadas de $CuInSe_2$, especialmente en procesos de deposición que implican múltiples etapas, como el tratamiento térmico y la pos-selenización. Estudiamos aquí la deposición de películas delgadas de $CuInSe_2$ mediante pulverización catódica por magnetrón de radiofrecuencia a partir de un blanco monofásico, variando la temperatura del sustrato entre 50 y 400 °C. La espectroscopía de fotoelectrones de rayos X (XPS) confirmó la presencia persistente de una capa superficial pobre en Cu en todas las temperaturas de deposición. Las películas depositadas por debajo de 200 °C resultaron amorfas y con deficiencia de cobre, mientras que a 200 °C y temperaturas superiores las películas mostraron una transición hacia una estructura policristalina tipo calcopirita, como lo evidenció la difracción de rayos X (XRD). Los tamaños de cristalito para las películas policristalinas depositadas

Citation: Montes-Monsalve J, *et al.* Study of the structural and optical properties of $CuInSe_2$ thin films obtained by RF sputtering as a function of the deposition temperature. Revista de la Academia Colombiana de Ciencias Exactas, Físicas y Naturales. 2025 Ago 25. doi: https://doi.org/10.18257/raccefyn.3225

Editor: Gabriel Téllez Acosta

***Corresponding autor:**
Jorge Montes-Monsalve;
jimontesm@unal.edu.co

Received: May 27, 2025
Accepted: July 8, 2025
Published on line: August 25, 2025

Revista de la Academia Colombiana de Ciencias Exactas, Físicas y Naturales. 2025
doi: https://doi.org/10.18257/raccefyn.3225

a 200 °C y 400 °C fueron de aproximadamente 10–12 nm. El análisis mediante espectroscopía de dispersión de energía de rayos X (EDS) reveló una disminución progresiva en el contenido de cobre, de ~20 % at. entre los 50 °C y los 200 °C a ~16 % at. a los 400 °C, en tanto que el contenido de indio se mantuvo casi constante y el de selenio aumentó ligeramente de 50 % at. a 56 % at. con el incremento de la temperatura. La espectroscopía UV-Vis mostró que el valor de la banda prohibida óptica (E_g) disminuy**ó** de 1,2 eV a 50 °C y 1,15 eV a 100 °C hasta aproximadamente 0,95–0,94 eV a 200 °C y 400 °C. Los resultados aportan información relevante sobre el papel de la temperatura del sustrato en la deposición de películas delgadas de $CuInSe_2$, lo que contribuye a los esfuerzos actuales por mejorar su desempeño en aplicaciones fotovoltaicas y optoelectrónicas.

Palabras clave: Seleniuros de cobre e indio; Película delgada; Espectroscopia de fotoelectrones de rayos X; Espectroscopia Raman; Difracción de rayos X; Optoelectrónica; Fotovoltaica.

Introduction

Chalcogenide materials belong to a significant family of semiconductors extensively used in photovoltaic and optoelectronic devices (**Kim *et al.***, 2021; **Torres *et al.,*** 2018). Over several decades, there has been intensive research to explore their unique properties and improve their manufacturing methods (**Chauhan *et al.***, 2018; **Cheng *et al.***, 2017; **Hodes & Cahen,** 1986; **Migliorato *et al.***, 1975; **Thomere *et al.***, 2022). These materials have gained significant attention due to their versatile applications and their potential for high-efficiency solar energy conversion (**Green *et al.***, 2024; **Jošt *et al.***, 2022; **Nanayakkara *et al.***, 2017; **Solhtalab *et al.***, 2022; **Wi *et al.***, 2018). Conventional silicon-based photovoltaic technology, while widely used, faces challenges such as high energy-intensive crystallization and purification processes, making it expensive and less sustainable (**Chauhan *et al.***, 2018). This has driven a shift towards second-generation solar cells based on heterojunction thin films, which offer cost-effectiveness and improved efficiency. Among the alternative materials explored, copper-based chalcopyrite compounds, such as $CuInSe_2$, have emerged as one of the most promising candidates for thin-film solar cells, particularly as an absorber layer in tandem solar cells where it can serve as the bottom junction (**Muzzillo *et al.***, 2018; **Sadono *et al.***, 2018; **Stanbery *et al.***, 2021; **Wang *et al.***, 2022).

$CuInSe_2$ is a ternary semiconductor of the I-III-VI_2 family, where I = Cu/Ag, III = In/Ga/Al, and VI = Se/S/Te, which exhibits a direct bandgap of approximately 1.05 eV, a high optical absorption coefficient (>10^5 cm^{-1}), excellent thermal stability, and superior conversion efficiency (**Hodes & Cahen**, 1986; **Migliorato *et al.***, 1975). Furthermore, $CuInSe_2$-based solar cells offer exceptional long-term stability, making them viable for commercial applications (**Thomere *et al.***, 2022). To enhance their photovoltaic performance, research efforts have focused on optimizing their electrical and optical properties through various deposition techniques, including metal-organic chemical vapor deposition, chemical bath deposition, chemical spray pyrolysis, co-evaporation, sputtering, atomic layer deposition, close-spaced vapor transport, and molecular beam epitaxy (**Li *et al.***, 2022; **Wang *et al.***, 2022; **Stanbery *et al.***, 2021; **Li *et al.,*** 2021; **Sadono *et al.***, 2018; **Cheng *et al.***, 2017). However, these methods often require expensive equipment and extreme processing conditions, limiting their scalability.

Electrodeposition has also been explored as a low-cost route for $CuInSe_2$, offering room-temperature processing and compositional control without vacuum equipment (**Hodes & Cahen**, 1986; **Chandran *et al.***, 2028). Although alternative routes like one-step and two-step electrodeposition are known, here we highlight radio-frequency magnetron sputtering, which provides better thickness uniformity and is more compatible with large-area manufacturing. Alkali- and transition-metal doping of $CuInSe_2$ can further tailor electrical or optical properties, for example, Li/Na improve carrier concentration, while Zn or Rb enhance grain growth and defect passivation (**Sharma *et al.***, 2023; **Malitckaya *et al.***, 2017), but here we focused exclusively on undoped films grown by RF magnetron sputtering. A comprehensive discussion of doped systems lies outside the scope of this work, but we cited key references for completeness.

Exceeding the photovoltaic performance beyond the single-junction Shockley-Queisser limit can be achieved using tandem solar cell structures, which employ two light-absorbing layers. Mathematical modeling suggests that, in a two-terminal tandem configuration under AM1.5 illumination, the top cell should have a bandgap (E_g) between 1.6 and 1.8 eV, while the bottom cell should have an E_g between 0.95 and 1.1 eV (**Fan *et al.***, 2011). $CuInSe_2$ (CIS) is a strong candidate for the bottom cell due to its bandgap of 1.0–1.04 eV (**Chauhan *et al.***, 2018; **Hodes & Cahen**, 1986). The highest efficiency reported for CIS solar cells currently stands at 15% (**Migliorato *et al.***, 1975). To further improve efficiency, Ga alloying has been used to form $Cu(InGa)Se_2$ (CIGS), with most high-efficiency devices featuring Ga/(Ga+In) concentrations of ~20–30% (**Thomere *et al.***, 2022). However, this increases the bandg ap above 1.1 eV, deviating from the optimal range for tandem solar cells. Consequently, alternative strategies for enhancing CIS-based solar cells with minimal Ga content are required.

Here, we focused on the synthesis and comprehensive characterization of $CuInSe_2$ thin films using RF magnetron sputtering at substrate temperatures ranging from 50°C to 400°C. Identifying the optimal temperature for high-quality $CuInSe_2$ formation is crucial, as it directly influences the film's structural, optical, and electronic properties. Our findings indicated that 200°C represents a critical threshold, as films deposited at this temperature exhibit a well-defined polycrystalline structure with minimal micro-strain, a dense morphology, and an ideal stoichiometry suitable for photovoltaic applications. Below 200°C, the films remain amorphous with poor crystallinity, while above 200°C, an increase in defect states and Cu deficiency affects the material's characteristics. By analyzing the optical, morphological, structural, and compositional properties of the films, we aimed to evaluate their potential applications beyond solar cells. Our results provide valuable insights into the effect of substrate temperature on $CuInSe_2$ thin films, contributing to the ongoing efforts to optimize their properties for photovoltaic and optoelectronic applications while emphasizing the importance of achieving high-quality film formation at relatively low deposition temperatures.

Experimental details

The thin CIS films were deposited at substrate temperatures ranging from 50°C to 400°C using a V4 magnetron sputtering system on soda-lime glass substrates. Before deposition, the glass substrates were sequentially cleaned in an ultrasonic bath using acetone, ethanol, and deionized water for 10 minutes each, and then dried with high-purity nitrogen gas. This cleaning process ensures the removal of organic contaminants and promotes better film adhesion. The films were sputtered from a commercial single-phase $CuInSe_2$ target in an Ar^+ atmosphere, at a working pressure of 0.7 Pa and a radio-frequency (RF) power of 35 W for 60 minutes. These deposition parameters were selected based on prior optimization experiments with Cu-based chalcopyrite materials, which showed that this pressure–power combination ensures a stable plasma, good uniformity, and minimal target damage while promoting adequate control over the film growth rate and phase composition.

We studied the following substrate temperatures: 50°C, 100°C, 200°C, and 400°C. We determined film thicknesses by profilometry with the following average values: 170 nm at 50°C, 240 nm at 100°C, 240 nm at 200°C, and 160 nm at 400°C. These thickness variations are attributed to the combined effects of adatom mobility and surface re-sputtering, which are known to increase with temperature in RF-sputtered systems. The deposited layers were characterized using various analytical techniques: X-ray diffraction (XRD); structural characterization was conducted using a Panalytical X'Pert MRD and MRD (XL) diffractometer operated at room temperature and equipped with a Cu Kα radiation source ($\lambda = 1.540562$ Å) at 30 kV and 15 mA, within a 2θ range of 20° to 60°. For Raman spectroscopy, the measurements were performed in backscattering geometry under normal incidence using a Raman Dilor XY LabRAM spectrometer. The system included an Olympus BX40 microscope with focusing capabilities of 10X, 20X, 50X, and 100X. Three

Revista de la Academia Colombiana de Ciencias Exactas, Físicas y Naturales. 2025
doi: https://doi.org/10.18257/raccefyn.3225

excitation laser wavelengths were used: 432 nm (blue), 532 nm (green), and 632 nm (red). For X-ray photoelectron spectroscopy (XPS), the surface composition analysis was carried out using a Thermo Scientific KAlpha X-Ray photoelectron spectrometer system equipped with an Al Kα X-ray source (1486.6 eV) and a base pressure of approximately $10^{-}9$ Pa.

Depth profiling was performed through superficial attrition with Ar+ ions at 3 kV. The relative atomic percentages of each element were quantified with the CASA XPS software employing a Lorentzian-Gaussian model for peak fitting. The optical properties of thin films were evaluated using a JASCO V-670 spectrometer, which operates in the ultraviolet to near-infrared (UV–NIR) range. Transmittance spectra were recorded and used to calculate the absorption coefficient based on the film thickness values obtained by profilometry. The optical bandgap energy (E_g) was extracted from Tauc plots assuming a direct allowed transition by extrapolating the linear portion of the $(\alpha h\nu)^2$ vs $h\nu$ curves. For the scanning electron microscopy (SEM), the morphological observation was conducted using a JEOL JSM7000 FE-SEM microscope with the following specifications: Resolution: 1.0 nm at 15 kV, 1.3 nm at 1 kV (GB), and 0.8 nm at 30 kV (SEM); accelerating voltage range: 100 V to 30 kV; magnification range: 25X to 1,000,000X. We took SEM images from the surface of each film to determine the morphology and analyze variations in relation to deposition parameters.

Results

X-ray analysis

The XRD measurements for each of the deposited films are shown in **Figure 1**. The films deposited at 50°C and 100°C exhibited amorphous characteristics, indicating a lack of long-range crystallinity. However, at 200°C and 400°C, the films transitioned into a structured form, demonstrating the development of a polycrystalline phase. A clear polycrystalline trend was observed, with three primary diffraction planes identified, two of which exhibited irregular shapes and low intensity, while the third presented a more distinct peak. The three diffraction planes were oriented at 2θ values of 26.64° (112), 44.20° (204/220), and 52.35° (116/132). These reflections correspond to $CuInSe_2$ with a tetragonal chalcopyrite structure, as verified in the JCPDS database card No. 089-5649, which confirmed that the deposited films maintained the expected crystallographic structure of the $CuInSe_2$ target material.

The crystallite size for the samples deposited at 200 °C and 400 °C was calculated and found to be approximately 10–12 nm. This indicates a moderate degree of grain growth as the deposition temperature increases, which plays a crucial role in determining the structural and optoelectronic properties of the films.

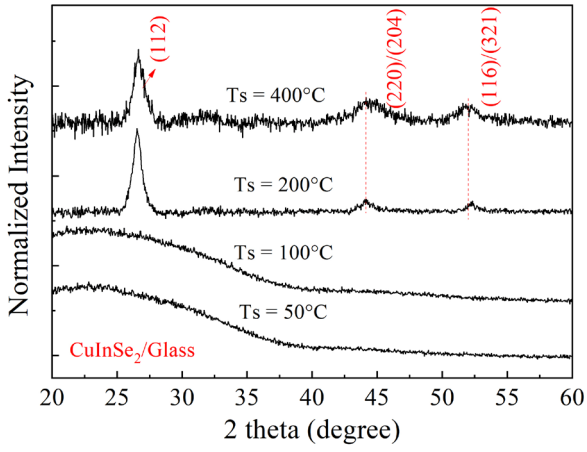

Figure 1. XRD of the $CuInSe_2$ deposited to Ts between 50 °C – 400 °C.

Raman analysis

A comparative analysis of the Raman spectra obtained from the deposited films at different substrate temperatures (**Figure 2**) revealed the presence of distinct optical vibrational modes. The main vibrational mode was observed at 173–176 cm^{-1}, while additional acoustic modes E and B_2 appeared at 211 cm^{-1} and 226 cm^{-1}, respectively. These vibrational features are consistent across all the analyzed films.

To assess the amount of material probed by the Raman laser, the penetration depth (δ) of the laser should be estimated using the following equation:

$$\delta=\lambda/4\pi k, \quad (1)$$

where λ represents the laser excitation wavelength and k is the extinction coefficient associated with the imaginary part of the complex refractive index $\hat{n} = n + ik$. For CIGS thin films, **Shafarman *et al.*** have reported k-values within the energy range of 0.75 – 4.6 eV at room temperature (**Paulson *et al.***, 2003). Based on ellipsometry measurements at specific wavelengths (500 nm and 1500 nm), a 632 nm excitation laser corresponds to an energy of 1.96 eV and an extinction coefficient of 0.45. By applying equation (1), the penetration depth was determined at 112 nm. Given that the film thickness varies depending on the substrate temperature, the laser penetrated more than 50% of all deposited films, ensuring a strong interaction with a significant volume of the material.

Upon closer examination of the spectra, at approximately 150 cm^{-1}, a weak Raman signal can be attributed to Cu-deficient $CuInSe_2$ structures, specifically ordered vacancy compounds (OVC) such as $CuIn_3Se_5$. This suggests that Cu-deficient phases are present on the film surface. However, while copper deficiency does not inherently imply an excess of selenium, in $CuInSe_2$-based photovoltaic devices, 'Cu-deficient and Se-rich' conditions are deliberately engineered to stabilize beneficial secondary phases such as $CuIn_3Se_5$, suppress the formation of selenium vacancies, and optimize both the band gap and p-type conductivity. This compositional strategy is crucial for achieving conversion efficiencies exceeding 20% in CIGS solar cells (**Ishizuka *et al.***, 2022). Additionally, we evaluated the full-width at half maximum (FWHM) as a function of the deposition temperature. Across most temperatures, the FWHM remained around 19 a.u., except for the film deposited at 400°C, which exhibited a slightly broader value of 22 a.u., an increase that is not particularly significant. The A_1 vibrational mode showed a shift from 176 cm^{-1} at 50°C to 173 cm^{-1} at

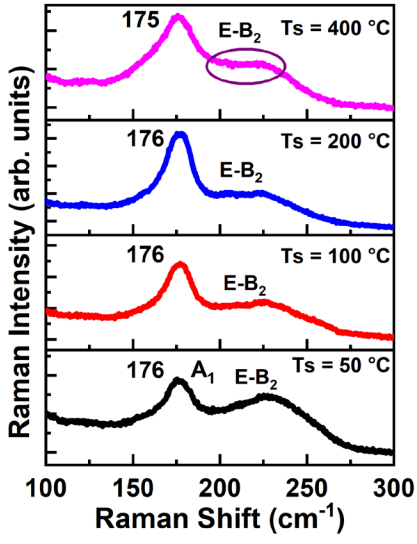

Figure 2. Raman spectra of the different samples deposited on glass substrates by RF magnetron sputtering at different substrate temperatures 50 °C- 400 °C.

Revista de la Academia Colombiana de Ciencias Exactas, Físicas y Naturales. 2025
doi: https://doi.org/10.18257/raccefyn.3225

400°C, a trend that has been previously reported in chalcopyrite-type materials. This shift has been attributed to changes in stoichiometry due to Cu vacancies, leading to the possible formation of $CuIn_{1.5}Se_2$ and $CuIn_3Se_5$ (**Maeda *et al.*,** 2016; **Xu *et al.***, 2004).

Previous studies have demonstrated that the broadening of the A_1 mode is not solely due to the presence of the weak signal around 150 cm^{-1}, but also to additional minor peaks observed in Raman spectra. We did not detect these peaks clearly in this study, but they have been linked to point defects and micro-stress effects induced by increasing deposition temperatures. Such structural modifications further confirm the strong dependence of $CuInSe_2$ film properties on substrate temperature.

EDS and SEM analysis

Energy dispersive spectroscopy (EDS) measurements were done to determine the elemental composition of the deposited films and verify whether the Cu deficiency contributed to the weak Raman signal observed at 150 cm^{-1}. The semi-quantitative analysis of a 0.5 μm^2 area (**Table 1**) provided insights into the elemental distribution at different substrate temperatures.

For films deposited at substrate temperatures between 50°C and 200°C, the atomic percentage of Cu remained approximately 20%. However, as the temperature increased to 400°C, the Cu content decreased to 16%. A similar trend was observed for In, but with minimal variation, fluctuating by only 2%, which falls within the instrumental error margin. The Se content, on the other hand, increased slightly with temperature, rising from 50% at 50°C to 56% at 400°C. This behavior suggests that the deficiency of Cu atoms led to an increase in Se concentration, as confirmed later by the XPS analysis, which indicated the presence of Se-Se bonds and SeO_2 formations. We believe these changes were responsible for the weak Raman signals at 150 cm^{-1} and the Raman shift from 176 cm^{-1} to 173 cm^{-1}, observed at higher deposition temperatures.

Besides the EDS analysis, we took scanning electron microscopy (SEM) images to examine the surface morphology of the films. The SEM images were captured at three different scales: 5 µm (magnification: 20Kx), 1 µm (magnification: 80Kx), and 500 nm (magnification: 150Kx) (**Figure 3**). The results indicated that the film deposited at 200°C exhibited distinct morphological characteristics compared to those deposited at other temperatures.

Films deposited at temperatures other than 200°C exhibited a smooth, compact, and uniform surface across the analyzed area, with no significant morphological variations. However, at 200°C, the surface morphology was noticeably different, characterized by a denser, rougher, and more granular texture. This suggested that 200°C was a critical threshold where $CuInSe_2$ thin films developed an optimal polycrystalline structure, affecting both their structural and optical properties.

XPS analysis

X-ray photoelectron spectroscopy (XPS) measurements were done to analyze the chemical composition, bonding states, and elemental depth distribution of the deposited $CuInSe_2$ thin films. The peak intensity in the XPS spectra indicated the relative surface concentration of elements, while the binding energy positions provided insights into their chemical states. Each element exhibited distinct electronic transitions when excited by X-rays.

Table 1. Elemental analysis of thin films as a function of temperature

Ts °C	Cu (at. %)	In (at. %)	Se (at. %)
50	21	29	50
100	19	27	54
200	21	26	53
400	16	28	56

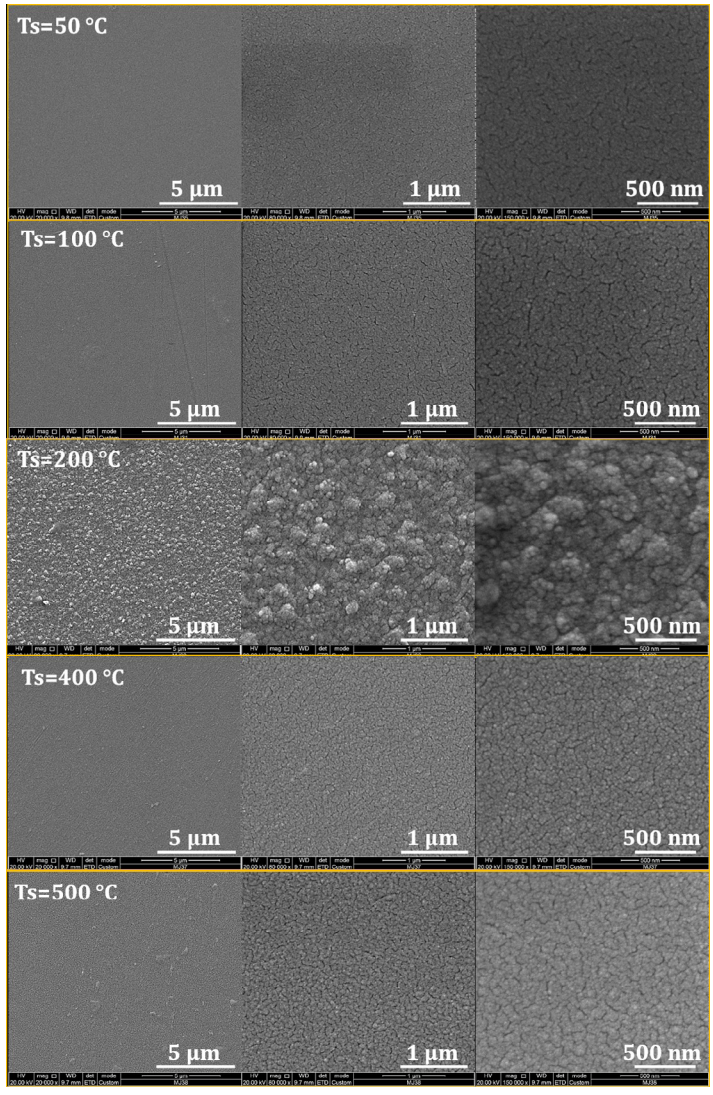

Figure 3. SEM-micrographs for the samples deposited at different substrate temperatures (50 °C, 100 °C, 200 °C, 400 °C, and 500 °C), and magnifications of 20,000X, 80,000X and 150,000X

Specifically, for Cu2p, the relevant transitions were $Cu2p_{5/2}$ and $Cu2p_{3/2}$; for In3d, they were $In3d_{5/2}$ and $In3d_{3/2}$, and for Se3d, the key transition was $Se3d_{3/2}$ (**Wanger**, 1979). To evaluate the reliability of the atomic percentage results derived from XPS, we considered the main sources of instrumental and methodological uncertainty: (i) repeatability of the measurements (≤ 1 % absolute); (ii) nominal accuracy from the RSF-based quantification method (± 1 % absolute); (iii) error propagation through the relative sensitivity factor model (~ 2 %), and (iv) signal variability induced by surface roughness and sputtering (estimated at ~ 3 %). The combined uncertainty was estimated by quadratic addition to be ≈ 4.1 %, which we rounded to a conservative value of ± 5 %. This value was represented in the form of error bars in the atomic composition plots by the XPS spectra of the analyzed films presented in **Figure 4**, divided into four sections:

- **Figure 4(a)**: The Cu2p transitions $Cu2p_{5/2}$ and $Cu2p_{3/2}$, associated with $CuInSe_2$, exhibited binding energies around 931.9 eV and 932.3 eV, respectively (**Wanger**, 1979; **Sobol**, 2021). The intensity variations of these peaks correlated with the Cu composition as a function of substrate temperature.

Revista de la Academia Colombiana de Ciencias Exactas, Físicas y Naturales. 2025
doi: https://doi.org/10.18257/raccefyn.3225

- **Figure 4(b)**: The In3d transitions $In3d_{5/2}$ and $In3d_{3/2}$ corresponded to $CuInSe_2$, with peaks appearing at approximately 444.7 eV (**Wanger**, 1979). The chemical composition of In was analyzed as a function of the deposition temperature.
- **Figure 4(c)**: The $Se3d_{3/2}$ transition was observed at 54 eV, corresponding to $CuInSe_2$, along with a secondary Se-Se bond at 55.1 eV (**Wanger**, 1979).

The right-hand side of **Figure 4** illustrates the atomic percentage evolution with substrate temperature; we applied the ± 5 % relative uncertainties only in these plots, as they derived from semi-quantitative RSF-based compositional analysis. No uncertainty estimation was applied to the peak fitting as such, which is used for qualitative interpretation of chemical states.

The obtained XPS values for Cu, In, and Se were consistent with values previously reported in the literature. However, slight variations in binding energies suggest oxidation effects, leading to the formation of In_2O_3 (indium oxide), SeO_2 (selenium oxide), and CuO (copper oxide). These oxidation states depend on substrate temperature. The presence of SeO_2 was predominantly detected in films deposited at 50°C to 200°C, indicating that selenium oxidation occurred primarily at low deposition temperatures (**Wanger *et al.***, 1979). As the temperature increased, SeO_2 presence diminished, suggesting that higher temperatures reduce oxidation effects. Conversely, CuO formation was notable at 200°C, coinciding with the temperature at which the highest Cu content was observed in the deposited films. Additionally, at 100 °C, some Cu(0) (zero-valence state) bonds were detected (**Wanger *et al.***, 1979). However, at other temperatures, the presence of Cu(0) or CuO remained unclear. Consequently, these contributions were not considered in peak fitting using the Lorentzian-Gaussian model, though their presence cannot be completely ruled out.

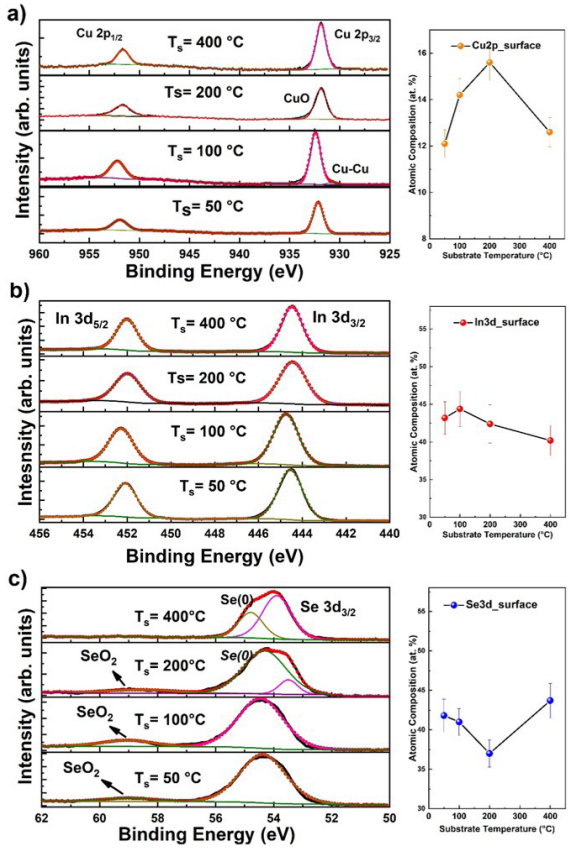

Figure 4. Fitted XPS Cu 2p, In 3d, and Se 3d spectra for the different films. On the right side, the concentration of Cu, In, and Se is observed as a function of the substrate temperature.

The comparison of EDS and XPS compositions revealed disparities in absolute atomic percentages because EDS probes the bulk whereas XPS is surface-sensitive. However, the trends remained consistent within the ± 5 % uncertainty window: Cu increased up to ~16 % at 200°C, then decreased; In remained stable around 40%, and Se content increased from 41% at 50°C to 44% at 400°C.

To further investigate the elemental distribution within the film depth, depth profiling was performed using Ar^+ ion sputtering. The depth profile spectra in **Figure 5** show elemental composition trends from the film surface (left) to a maximum etching time of 40 seconds (right). Due to the short etching duration, the depth profile primarily captured near-surface elemental variations. A clear Cu deficiency trend was observed across different depths, reinforcing the hypothesis that Cu vacancies increase with deposition temperature, affecting the overall stoichiometry of the $CuInSe_2$ thin films.

UV-Vis analysis

The optical properties of the deposited $CuInSe_2$ films were assessed by measuring transmittance in the UV-visible and near-infrared ranges. The optical bandgap energy (E_g) was determined as a function of substrate temperature (**Figure 6**). The calculated E_g values were:

- 1.2 eV for Ts = 50°C
- 1.15 eV for Ts = 100°C
- 0.95 eV for Ts = 200°C
- 0.94 eV for Ts = 400°C

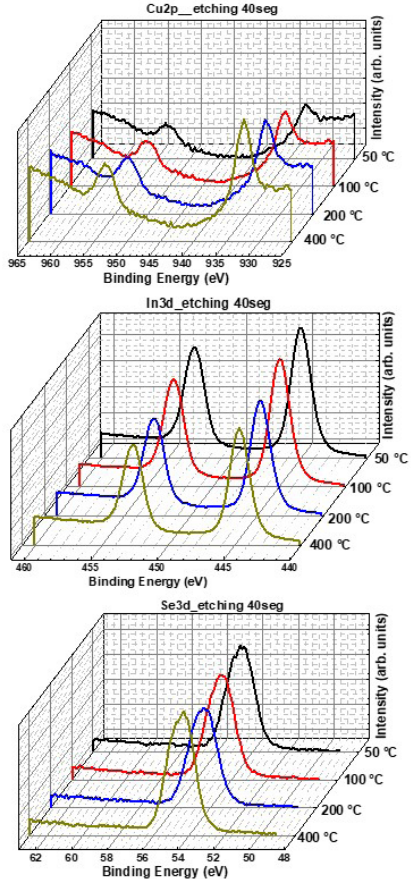

Figure 5. Cu 2p, In 3d, and Se 3d XPS spectra on the etched CIS thin films

Revista de la Academia Colombiana de Ciencias Exactas, Físicas y Naturales. 2025
doi: https://doi.org/10.18257/raccefyn.3225

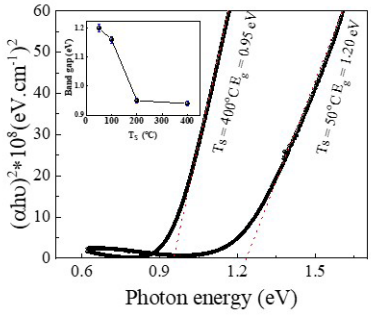

Figure 6. Tauc Plots of $(\alpha*h\nu)^2$ vs hν for the co-sputtered samples at 50°C and 400°C. The inset shows the behavior of the bandgap as a function of the substrate temperature.

To assess the accuracy of the extracted E_g values, we conducted an uncertainty analysis. The main sources of error included the spectral resolution of the JASCO V-670 spectrometer (±1 nm), the selection of the linear fitting region in the Tauc plot, and the reproducibility across repeated measurements. Considering these contributions, we estimated a conservative standard deviation of ±0.03 eV for all E_g values that are displayed in the inset of the figure. Bandgap differences greater than 0.05 eV were considered significant within this error margin. The results indicated that E_g remained constant for deposition temperatures above 200°C, while a slight variation was observed at 50°C and 100°C. The difference at 50°C may be attributed to the amorphous nature of the film, as confirmed by XRD analysis, where a lack of crystallinity was observed.

Despite the presence of oxides and structural defects acknowledged throughout the study, the measured E_g values aligned with those reported in the literature for $CuInSe_2$ (**Neumann**, 1986). This suggested that the ternary compound was successfully deposited, even with the Cu deficiency (**Zhang *et al.***, 1998). Previous reports indicated that E_g values between 1.2 eV and 1.3 eV are typical for Cu-deficient compounds such as $CuIn_3Se_5$ and $CuIn_5Se_8$ (**Maeda *et al.***, 2016) and reported, besides, a phase mixture where the Cu-poor phase (ordered defect compound, ODC) forms on the film surface, while $CuInSe_2$ remains in the bulk (**Fan *et al.***, 2011; **Maeda *et al.***, 2016). This observation supports the elemental composition obtained in this study, reinforcing the conclusion that the deposited films corresponded to $CuInSe_2$ with an intrinsic Cu deficiency that led to the generation of Cu vacancies (VCu) on the surface. Recent first-principles simulations (**Mahraj *et al.***, 2024) using DFT with the modified Becke–Johnson potential (mBJ) provide valuable insights into the electronic and optical structure of $CuInSe_2$ and related chalcopyrite compounds. Their calculations show that the upper valence band is dominated by Cu 3d orbitals, while the conduction band edge mainly consists of In 5s and Se 4p states. This electronic structure explains the strong direct transitions observed near the Γ point, resulting in high absorption coefficients ($\sim 10^5\ cm^{-1}$) in the visible range—in good agreement with our experimental UV–Vis data. Moreover, their analysis highlights how structural distortions (e.g., anion displacement) and Cu-vacancy formation can reduce the bandgap by introducing localized band-tail states. This supports our interpretation that, despite the formation of Se-rich phases or Cu-deficient surface layers, the observed optical bandgap ($E_g \approx 0.94$–1.20 eV) remained consistent with theoretical bulk values, since the main transitions were governed by the defect-tolerant Cud–Sep hybridized states.

We concluded that the substrate temperature directly influenced the Cu content in the films. Higher deposition temperatures led to an increase in Cu vacancies (V_{Cu}) on the material's surface, as confirmed by the XPS analysis. However, despite the Cu deficiency, the optical bandgap (E_g) remained unaffected by the temperature variation. This finding suggests that the electronic structure of $CuInSe_2$ was preserved, even when Cu vacancies were present, reinforcing its stability and applicability in photovoltaic and optoelectronic devices.

Finally, the experimental results obtained in this study provide valuable insights into the effect of substrate temperature on the structural, morphological, optical, and compositional properties of $CuInSe_2$ thin films. It has been demonstrated that the substrate temperature plays a crucial role in controlling crystallinity, elemental distribution, and defect formation, ultimately influencing the film's behavior in photovoltaic and optoelectronic applications. A key observation from the XRD and Raman analyses is the transition from an amorphous structure at low temperatures (50°C and 100°C) to a well-defined polycrystalline phase at 200°C and above. This transition was accompanied by an increase in crystallite size, indicating improved structural order. However, films deposited at 400°C exhibited an increase in Cu vacancies, as evidenced by XPS and EDS measurements, leading to a slight shift in Raman vibrational modes and the formation of minor defect states. Substrate temperature had a strong impact on the structure, morphology, roughness, and optical properties of $CuInSe_2$ films. Some studies report that films deposited at 200°C exhibit optimal phase formation, surface morphology, and roughness, leading to superior electrical and optical performance (**Yan *et al.***, 2011).

The UV-Vis analysis confirmed that the optical bandgap (E_g) remained stable for films deposited at temperatures above 200°C, with a slight deviation at lower temperatures due to amorphous content and structural disorder. Notably, despite the presence of Cu vacancies, the bandgap remained within the expected range for $CuInSe_2$, reinforcing its stability as a semiconductor material. Surface morphology, as observed in SEM images, revealed that films deposited at 200°C exhibited a dense, compact, and uniform grain structure, distinguishing them from those deposited at other temperatures. Films deposited at higher temperatures showed increased surface roughness, likely due to enhanced atomic mobility and Cu depletion, which may introduce additional defect states impacting electrical properties. These findings emphasize the importance of achieving high-quality $CuInSe_2$ film formation at relatively low deposition temperatures. The optimal substrate temperature of 200°C ensured a well-defined polycrystalline structure, minimal defect formation, and an ideal balance of composition and morphology. This makes $CuInSe_2$ an excellent candidate for photovoltaic absorbers in thin-film solar cells in tandem configurations, as well as for applications in optoelectronic devices where precise control over structural and electronic properties is required.

To conclude, our study contributes to the ongoing efforts to optimize $CuInSe_2$ deposition processes, providing a deeper understanding of how substrate temperature influences film formation. Future research should explore electrical transport properties, defect engineering strategies, and potential passivation techniques to further enhance the material's efficiency and stability in energy conversion technologies.

A possible limitation of the study is the surface sensitivity of XPS (~5–10 nm), which may over-emphasize Cu-vacancy formation and oxide species confined to the outermost layers while under-representing bulk composition. Complementary depth-profiling or hard-XPS measurements would help disentangle true bulk stoichiometry from surface artifacts. In addition, alkali-metal passivation, particularly in-situ or post-deposition Na incorporation, is known to decrease grain-boundary recombination and stabilize Cu-poor surfaces in chalcopyrite. Future experiments combining controlled Na doping, soft anneals, and in-depth chemical profiling will be essential to optimize both the electronic quality and long-term stability of RF-sputtered $CuInSe_2$ absorber layers.

Conclusions

Systematic variation of the substrate temperature during RF magnetron sputtering from a single-phase $CuInSe_2$ target revealed a critical threshold around 200°C: only above this point did the adatom mobility become high enough to promote long-range diffusion, grain coalescence, and the emergence of a well-defined chalcopyrite lattice. Films grown at $\geq$ 200°C showed polycrystalline domains (10–12 nm), minimal micro-stress, and a dense surface free of inter-granular voids, making them promising absorber layers for photovoltaic or other optoelectronic devices.

Revista de la Academia Colombiana de Ciencias Exactas, Físicas y Naturales. 2025
doi: https://doi.org/10.18257/raccefyn.3225

At higher temperatures, however, differential atomic mobility and surface re-sputtering favored the preferential loss of Cu species, increasing the concentration of Cu vacancies (V_{Cu}) at the film surface, as confirmed by the progressive Cu depletion detected by XPS. Despite this surface Cu deficiency, the optical band-gap ($E_g \approx 0.94 – 1.20$ eV) remained essentially unchanged within the ± 0.03 eV experimental uncertainty, suggesting that V_{Cu} states induce only shallow band-tailing rather than a shift in the fundamental gap.

Raman spectroscopy supports this interpretation: the dominant A1 mode of $CuInSe_2$ was present at all temperatures, whereas the weak 150 cm^{-1} signal associated with ordered-vacancy compounds became slightly more pronounced at ≥ 200°C, in agreement with an increased V_{Cu} population. Overall, the data indicated that atomic-scale transport processes at elevated substrate temperatures simultaneously enhanced crystallinity and promoted Cu-vacancy formation, defining an optimal growth window near 200°C that balanced structural quality with compositional integrity.

Acknowledgements

The authors would like to thank Dr. S. Velázquez for XPS measurements and A. Tavira-Fuentes, G. Casados-Cruz, M. Galván, and G. López Fabián of SEES-CINVESTAV-IPN for the different characterizations of the films. A. Pulzara expresses gratitude to the FCEN for granting the sabbatical year.

Author contributions

J.I.M-M: Methodology, validation, formal analysis, investigation, data curation, writing of original draft, review & editing, visualization, and conceptualization; R.B-C: Methodology, validation, visualization in structure presented in previous formal analysis, writing of original draft; A. M-A: Methodology, validation, formal analysis, investigation, conceptualization, writing of original draft, review and editing, supervision; A. P-M: Conceptualization, methodology, validation, formal analysis, resources, writing of original draft, writing review and editing, project administration, funding acquisition.

Conflicts of interest

The authors declare that they have no competing financial interests or personal relationships that could have influenced the work reported in this paper.

References

Chandran R. & Mallik A. (2018). Electrodeposition of near stoichiometric $CuInSe_2$ thin films for photovoltaic applications. *IOP Conference Series: Materials Science and Engineering, 338*, 012018. https://doi.org/10.1088/1757-899X/338/1/012018

Chauhan S.M., Chaki S.H., Deshpande M.P., Malek T.J., Tailor J.P. (2018). Thermal Decomposition Study on $CuInSe_2$ Single Crystals. *International Journal of Thermophysics*, *39*, 18. https://doi.org/10.1007/s10765-017-2341-4

Cheng K.W., Jhang H.J., Li C.T., Ho K.C. (2017). Solution-growth-synthesized Cu (In,Ga) Se_2 nanoparticles in ethanol bath for the applications of dye-sensitized solar cell and photoelectrochemical reaction. *Journal of the Taiwan Institute of Chemical Engineers*, *74*, 136-145. https://doi.org/10.1016/J.JTICE.2017.02.010

Cheng Y.S., Wang N.F., Tsai Y.Z., Lin J.J., Houng M.P. (2017). Investigation of $CuInSe_2$ nanowire arrays with core–shell structure electrodeposited at various duty cycles into anodic alumina templates. *Applied Surface Science*, *396*, 631-636. https://doi.org/10.1016/J.APSUSC.2016.10.207

Fan P., Liang G.X., Cai X.M., Zheng Z.H., Zhang D.P. (2011). The influence of annealing temperature on the structural, electrical and optical properties of ion beams sputtered $CuInSe_2$ thin films. *Thin Solid Films*, *519*, 5348-5352. https://doi.org/10.1016/J.TSF.2011.02.036

Green M.A., Dunlop E.D., Yoshita M., Kopidakis N., Bothe K., Siefer G., Hao X., Jiang J. Y. (2024). Solar cell efficiency tables (Version 60). *Progress in Photovoltaics: Research and Applications, 33*, 3-15. https://doi.org/10.1002/pip.3867

Hodes G. & Cahen D. (1986). Electrodeposition of $CuInSe_2$ and $CuInS_2$ films. *Solar Cells*, *16*, 245-254. https://doi.org/10.1016/0379-6787(86)90088-8

Ishizuka S., Nishinaga J., Beppu K., Maeda T., Aoyagi F., Wada T., Yamada A., Chantana J., Nishimura T., Minemoto T., Monirul Islam M., Sakurai T., Terada. (2022). Physical and chemical aspects at the interface and in the bulk of $CuInSe_2$-based thin-film photovoltaics. *Journal Physical Chemistry Chemical Physics, 24,* 1262. https://doi.org/10.1039/D1CP04495H

Jošt M., Köhnen E., Al-Ashouri A., Bertram T., Tomšič Š., Magomedov A., Kasparavicius E., Kodalle T., Lipovšek B., Getautis V., Schlatmann R., Kaufmann C.A., Albrecht S., Topič M. (2022). Perovskite/CIGS Tandem Solar Cells: From Certified 24.2% toward 30% and beyond. *ACS Energy Letters*, *7*, 1298-1307. https://doi.org/10.1021/acsenergylett.2c00274

Kim S.T., Yoo J.S, Lee M.W., Jung J.W., Jang J.H. (2022). $CuInSe_2$-Based Near-Infrared Photodetector. *Applied Science*, *12*, 92. https://doi.org/10.3390/APP12010092

Li L., Chen Y., Lv Z., Yin N.Q., Li S., Wang K., Li P. (2022). In situ one-step synthesis of $CuInS_2$ thin films with different morphologies and their optical properties. *Journal of Materials Science: Materials in Electronics*, *33*, 2995-3001. https://doi.org/10.1007/S10854-021-07499-6

Li L., Li M., Li P. (2021). Cu $(In,Ga)S_2$ nanowire arrays: Self-templated synthesis and application for photoelectrochemical water splitting. *Materials Characterization*, *172*, 110900. https://doi.org/10.1016/J.MATCHAR.2021.110900

Mahraj I. & Ptok A. (2024). First-principles investigations of structural, electronic and optical properties of ternary chalcopyrite semiconductors $CuInY_2$. (Y = S, Se and Te). *Computational Condensed Matter*, *40*. E 00935. https://doi.org/10.1016/j.cocom.2024.e00935

Malitckaya M., Komsa H., Havu V., Puska M. J. (2017). Effect of Alkali Metal Atom Doping on the $CuInSe_2$-Based Solar Cell Absorber. *The Journal of Physical Chemistry C*, *121*, 29, 15516-15528. https://doi.org/10.1021/acs.jpcc.7b03083

Maeda T., Gong W., Wada T. (2016). Crystallographic and optical properties and band structures of $CuInSe_2$, $CuIn_3Se_5$, and $CuIn_5Se_8$ phases in Cu-poor Cu_2Se-In_2Se_3 pseudo-binary system. *Japanese Journal of Applied Physics*, *55*, 04ES15. https://doi.org/10.7567/JJAP.55.04ES15

Migliorato P., Shay J.L., Kasper H.M. (1975). Electrical properties and luminescence of $CuInSe_2$. *Journal of Electronic Materials*, *4*, 209-222. https://doi.org/10.1007/BF02655402

Muzzillo C.P., Li J. V., Mansfield L.M., Ramanathan K., Anderson T.J. (2018). Surface and bulk effects of K in highly efficient $Cu_{1-x}K_xInSe_2$ solar cells. *Solar Energy Materials and Solar Cells*, 185 45-53. https://doi.org/10.1016/J.SOLMAT.2018.05.013

Nanayakkara S.U., Horowitz K., Kanevce A., Woodhouse M., Basore P. (2017). Evaluating the economic viability of CdTe/CIS and CIGS/CIS tandem photovoltaic modules. *Progress in Photovoltaics*, *25*, 271-279. https://doi.org/10.1002/PIP.2849

Neumann H. (1986). Optical properties and electronic band structure of $CuInSe_2$, *Solar Cells*, *16*, 317-333. https://doi.org/10.1016/0379-6787(86)90092-X

Paulson P.D., Birkmire R.W., Shafarman W.N. (2003). Optical characterization of $CuIn_{1-x}Ga_xSe_2$ alloy thin films by spectroscopic ellipsometry. *Journal of Applied Physics, 94*, 879-888. https://doi.org/10.1063/1.1581345

Sadono A., Hino M., Nakada K., Yamada A. (2018). Effect of an additional Cu-deficient layer deposition on alkali treated $Cu(In,Ga)Se_2$ solar cells deposited at low temperature. *Solar Energy Materials and Solar Cells*, *184*, 67-72. https://doi.org/10.1016/J.SOLMAT.2018.04.030

Sharma S., Khan K., Soni M., Ahuja U., Soni A., Sahariya J. (2023). Investigation of electronic and optical properties of alkali atom doped CuInSe2 using density functional theory. *Physica Scripta, 98* 085927. https://doi.org/10.1088/1402-4896/ace489

Sobol P.E., Nelson A.J., Schwerdtfeger C.R., Stickle W.F., Moulder J.F. (2021). Single Crystal $CuInSe_2$ Analysis by High Resolution XPS. *Surface Science Spectra*, *1* 393-397. https://doi.org/10.1116/1.1247638

Solhtalab N., Mohammadi M.H., Eskandari M., Fathi D. (2022). Efficiency improvement of half-tandem CIGS/perovskite solar cell by designing nano-prism nanostructure as the controllable light trapping. *Energy Reports*, *8,* 1298-1308. https://doi.org/10.1016/J.EGYR.2021.12.038

Stanbery B.J., Abou-Ras D., Yamada A., Mansfield L. (2021). CIGS photovoltaics: reviewing an evolving paradigm. J*ournal of Physics D: Applied Physics*, *55*, 173001. https://doi.org/10.1088/1361-6463/AC4363

Thomere A., Barreau N., Stephant N., Guillot-Deudon C., E. Gautron, Caldes M.T., Lafond A. (2022). Formation of $Cu(In,Ga)S_2$ chalcopyrite thin films following a 3-stage co-evaporation process. *Solar Energy Materials and Solar Cells*, *237,* 111563. https://doi.org/10.1016/J.SOLMAT.2021.111563

Torres-Jaramillo S., Morales-Acevedo A., Bernal-Correa R., Pulzara-Mora A. (2018). Optimizing two and four-terminal $CuGaSe_2$/$CuInGaSe_2$ tandem solar cells for achieving high efficiencies. *Optik, 175*, 71-77. https://doi.org/10.1016/J.IJLEO.2018.08.124

Wang C., Zhuang D., Zhao M., Li Y., Tong H., Wang H., Wei J., Gong Q. (2022). High-performance sub-micron CIGSSe solar cells optimized for sodium doping by adjusting diffusion barriers. *Chemical Engineering Journal*, *439,* 135713. https://doi.org/10.1016/J.CEJ.2022.135713

Wanger C. D., Riggs W. M., Davis L. E., Moulder J. F., Muilenberg G. E. (1979). Handbook of X-ray Photoelectron Spectroscopy, Perkin-Elmer Corp., Physical Electronics Division, Eden Prairie. https://doi.org/10.1002/SIA.740030412

Wi J.H., Han W.S., Lee W.J., Cho D.H., Yu H.J., Kim C.W., Jeong C., Yun J.H., Kim C.I., Chung Y.D. (2018). Spectral Response of $CuGaSe_2$/$Cu(In,Ga)Se_2$ Monolithic Tandem Solar Cell with Open-Circuit Voltage over 1 V. *IEEE Journal of Photovoltaics*, *8,* 840-848. https://doi.org/10.1109/JPHOTOV.2018.2799168

Xu C.M., Xu X.L., Xu J., Yang X.J., Zuo J., Kong N., Huang W.H., Liu H.T. (2004). Composition dependence of the Raman A1 mode and additional mode in tetragonal Cu–In–Se thin films. *Semiconductor Science and Technology*, *19* 1201. https://doi.org/10.1088/0268-1242/19/10/006

Yan Z., Ji X, Li M., Mi Y. (2011). Effect of substrate temperature on properties of $CuInSe_2$ thin films deposited by magnetron sputtering. *Advanced Materials Research*, 287-290, 2131-2135. https://doi.org/10.4028/www.scientific.net/AMR.287-290.2131

Zhang S.B., Wei S., Zunger A. (1998). Defect physics of the $CuInSe_2$ chalcopyrite semiconductor. *Physical Review B, 57*, 9642-9656. https://doi.org/10.1103/PhysRevB.57.9642

Highlights

- $CuInSe_2$ single target and unique step deposition to obtain $CuInSe_2$
- Structure, morphology, optical, and surface analysis have been made to understand the film's nature.
- The XPS and Raman measurements revealed clearly the effect Cu deficient composition has on a surface independent of substrate temperature and the nature of the thin films.
- In the process to deposit a thin film, the temperature below 200°C generated amorphous material with Cu-deficient content.
- Despite the lack of Cu atoms in the films deposited in this study, it has been shown that E_g does not seem to depend on a deposition temperature above 200°C.